FISEVIED

Contents lists available at ScienceDirect

Journal of the Mechanical Behavior of Biomedical Materials

Journal of Ind.
Mechanical Behavior of Biomedical Materials

journal homepage: www.elsevier.com/locate/jmbbm

Mechanical characterization of *Xenopus laevis* oocytes using atomic force microscopy

Tatiana Kardashina ^a, Elba E. Serrano ^b, John A. Dawson ^c, Borys Drach ^{a,*}

- ^a Department of Mechanical and Aerospace Engineering, New Mexico State University, Las Cruces NM, USA
- ^b Department of Biology, New Mexico State University, Las Cruces NM, USA
- ^c Department of Economics, Applied Statistics, and International Business, New Mexico State University, Las Cruces NM, USA

ABSTRACT

Mechanical properties are essential for the biological activities of cells, and they have been shown to be affected by diseases. Therefore, accurate mechanical characterization is important for studying the cell lifecycle, cell-cell interactions, and disease diagnosis. While the cytoskeleton and actin cortex are typically the primary structural stiffness contributors in most live cells, oocytes possess an additional extracellular layer known as the vitelline membrane (VM), or envelope, which can significantly impact their overall mechanical properties. In this study, we utilized nanoindentation via an atomic force microscope to measure the Young's modulus of *Xenopus laevis* oocytes at different force setpoints and explored the influence of the VM by conducting measurements on oocytes with the membrane removed. The findings revealed that the removal of VM led to a significant decrease in the apparent Young's modulus of the oocytes, highlighting the pivotal role of the VM as the main structural component responsible for the oocyte's shape and stiffness. Furthermore, the mechanical behavior of VM was investigated through finite element (FE) simulations of the nanoindentation process. FE simulations with the VM Young's modulus in the range 20–60 MPa resulted in force-displacement curves that closely resemble experimental in terms of shape and maximum force for a given indentation depth.

1. Introduction

Biological cells are constantly subjected to mechanical forces throughout their lifecycle. Cells have the remarkable ability to sense and respond to these mechanical stimuli, translating them into electrical or chemical signals (Jaalouk and Lammerding, 2009). The mechanical properties of cells including the forces acting on them from both external and internal environments, play a crucial role in many biological processes such as development, growth, and differentiation (Ayad et al., 2019), (Wozniak and Chen, 2009).

Previous research has shown that certain mechanical properties, such as elasticity and viscoelasticity, differ between unhealthy and healthy cells. These differences can serve as indicators of specific diseases. For example, the analysis of metastatic adenocarcinoma cells revealed that malignant cells exhibit a significantly lower Young's modulus compared to healthy cells (Cross et al., 2007). In another study, pancreatic cancer cells showed significant decrease in Young's modulus (Suresh, 2007). Xu et al. (2012) showed that non-malignant immortalized ovarian surface epithelial cells have higher Young's modulus than ovarian cancer cells and in a case of malaria, infected red blood cells show a 10-fold increase in rigidity (Suresh et al., 2005). Moreover, interest in reproductive technologies has directed attention to the

mechanical properties of oocytes that underlie successful fertilization, implantation, and embryonic development (Elad et al., 2020), (Shah et al., 2018), (Kort and Behr, 2017). Viscoelasticity has been shown to correlate with oocyte viability in mice and humans (Yanez et al., 2016), sparking interest in methods that can identify mechanically competent oocytes. Atomic force microscopy (AFM) is emerging as a potential minimally-invasive diagnostic tool for oocyte characterization with application for the reproductive pipeline, for example, following cryopreservation (Battistella et al., 2022).

It is important to note that cells are not homogeneous, and their mechanical properties and shape are governed by their structure, especially the actin cortex (Sackmann, 1994), (Salbreux et al., 2012). Numerous studies have been conducted to measure the mechanical properties of animal cells and explore their effects on various biological processes. However, the reported range of apparent Young's moduli in the literature varies significantly, spanning from 0.1 kPa to 100 kPa (Cross et al., 2007), (Braet et al., 1998), (Mathur et al., 2001), (Dimitriadis et al., 2002), (Codan et al., 2013). This wide variation can be attributed to different experimental techniques (Wu et al., 2018), (Daza et al., 2019), experiment protocols, types of cells (Rosenbluth et al., 2006), data processing and other factors. Even experiments conducted with the same protocol gave variability in the results due to errors

E-mail address: borys@nmsu.edu (B. Drach).

^{*} Corresponding author.

during calibration of the AFM (Schillers et al., 2017).

The cell poking approach was first developed in the early 1980s, where small tip was used to measure the cell response under applied force (Daily et al., 1984), (McConnaughey and Petersen, 1980), (Petersen et al., 1982). Subsequently, in 1986 AFM was developed (Gavara, 2017), employing a similar technique. Since then, AFM has been broadly used for cell imaging and the measurement of mechanical properties. AFM uses a small tip attached to a flexible cantilever to interact with a sample. Deflection of the cantilever is tracked by a laser beam and a photodetector able to detect the laser beam. Bio AFM can apply small forces in the magnitude of pN (Méndez-Vilas and Díaz, 2010), (Zhou et al., 2021) to soft biological samples enabling precise measurements in either air or liquid environments. Bio AFM has been used to investigate Young's modulus of various cell types. Rico et al. demonstrated that alveolar epithelial cells exhibited higher values when probed with a pyramidal tip (~0.9 kPa) compared to a spherical tip (~0.5 kPa) (Rico et al., 2005). MCF-10 A normal breast cells showed a Young's modulus value of ~5 kPa, whereas MCF-7 cancerous breast cells exhibited ~3.5 kPa (Li et al., 2018). The undifferentiated multipotent mesenchymal stromal/stem cells displayed a Young's modulus of ~2 kPa, which increased to ~12 kPa as the cells underwent differentiation (Yen et al., 2020). Another investigation utilizing AFM revealed that cardiac cells exhibited the highest stiffness (~100 kPa), followed by skeletal muscle cells (~25 kPa), while endothelial cells were found to be the softest (\sim 1.4–7 kPa) (Mathur et al., 2001).

The Xenopus laevis oocyte (egg) is a large, readily accessible cell that is widely used to study cellular, molecular, physiological, and developmental processes (Mowry, 2020). Oocytes are surrounded by a vitelline membrane (VM) that forms a protective barrier and prevents multiple sperm from fusing with the egg. The VM of Xenopus oocytes comprises a thick layer of protein fibers approximately 1 μm in thickness (Tian et al., 1997), (Larabell and Chandler, 1989). Although AFM has been extensively utilized for probing the mechanical properties of cells, to the best of our knowledge, AFM-based mechanical property measurements with intact live Xenopus oocytes are lacking. While the mechanical properties of intact Xenopus oocytes have not been extensively investigated via nanoindentation methods, oocytes have been the focus of biomechanics studies using other approaches. Valentine et al. (2005) investigated mechanical properties of *Xenopus* egg cytoplasmic extracts using a rheometer and found the elastic modulus to be in the range of 2–10 Pa, and loss modulus in the range of 0.5–5 Pa. Kelly et al. (1997) estimated specific elastance of *Xenopus* oocytes with and without the VM by measuring intracellular pressure and cell volume during osmotic swelling using a servo-null pressure transducer. The authors obtained values of 0-5.59 kPa for intact oocytes and 0.15-1.03 kPa for oocytes without the VM. Previous studies with biological samples such as T-lymphocytes, isolated nuclei and chondrocytes have shown differences between mechanical property measurements obtained by nanoindentation via AFM and micropipette aspiration (Daza et al., 2019), (Dahl et al., 2005), (Darling et al., 2006).

This paper analyzes the influence of the VM on the apparent elastic $\,$

properties of *Xenopus* oocytes. AFM was used to collect experimental data at the animal and vegetal poles on the oocytes with and without the VM. The effects of indentation force and contact model for fitting force-displacement curves (Hertz vs JKR) on the apparent Young's modulus of the oocytes were evaluated.

2. Materials and methods

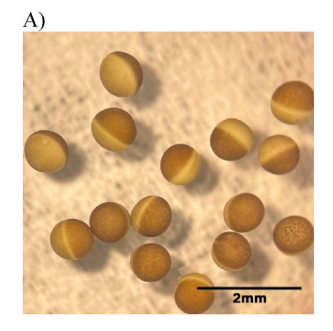
2.1. Samples

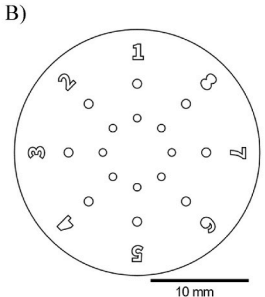
Unfertilized defolliculated stage V/VI *Xenopus laevis* oocytes (Fig. 1A) were ordered from Ecocyte Bioscience (Austin, TX, USA; RRID: SCR_024430). Live oocytes were maintained at 4–6 °C according to the vendor guidelines. For indentation of oocytes without the VM, the membrane was removed from oocytes in Normal Frog Ringer (NFR; Ecocyte Bioscience; Austin, TX, USA; RRID:SCR_014773) using two pairs of forceps following immersion (10 min) in Vitelline Removal Solution (VRS; Ecocyte Bioscience; Austin, TX, USA; RRID:SCR_014773). VM-free oocytes experiments were completed the day the membrane was removed.

2.2. Bio-AFM equipment setup and calibration procedures

Imaging and force spectroscopy measurements were acquired with a Bio-AFM comprising a NanoWizard® 4 XP Atomic Force system (Bruker Nano, Inc., Santa Barbara, CA) configured for an inverted Olympus IX73 fluorescence microscope (Olympus America Inc., Waltham MA) with an Andor Zyla 5.5 sCMOS scientific camera (Oxford Instruments, Abingdon, England), and the Bruker JPK SPM software. The Bio-AFM was mounted on an Accurion i4 active vibration isolation system (Park Systems, Inc, Santa Clara, CA) and housed within a JPK Acoustic Enclosure (Bruker Nano, Inc., Santa Barbara, CA). The JPK Manual Precision Stage was maintained at room temperature (25–27 °C) and configured to hold 35 mm petri dishes (TPP Techno Plastic Products AG, Switzerland).

Optimization experiments were undertaken with an array of cantilevers with varying spring constants ranging from 0.006 to 0.45 N/m, with the purpose of identifying the most suitable cantilever for proper indentation (data not shown). It was observed that probes with spring constants 0.2 N/m and higher yielded proper indentation results (see discussion in Section 3.2.1). Elastic properties presented in the results section were determined using cantilevers with a nominal spring constant of 0.25 N/m, cylindrical tip and 10-µm end radius (SAA-SPH-10UM, Bruker, Camarillo, CA). QI images were acquired using ultrasharp tip cantilever with 1-nm end radius, and nominal spring constant of 0.35 N/m (PEAKFORCE-HIRS-FA, Bruker, Camarillo, CA). After each use, probes were immersed in 3% Tergazyme® Enzyme-Active Powdered Detergent (Alconox, Inc; White Plains, NY) solution for 30-60 min, rinsed in distilled water, and allowed to air dry. The shape and dimensions of the cantilever SAA-SPH-10UM were inspected with a Hitachi SEM (Tokyo, Japan) as shown in Fig. 2. Observed radius





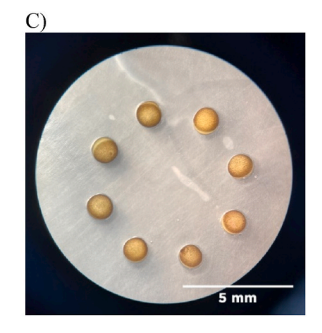


Fig. 1. A) Live unfertilized *Xenopus* oocytes (stage V/VI): animal pole is the darkly pigmented and vegetal pole is lightly pigmented B) diagram of the cell holder designed for immobilizing cells during nanoindentation, C) live *Xenopus* oocytes placed in the inner circles of the holder.

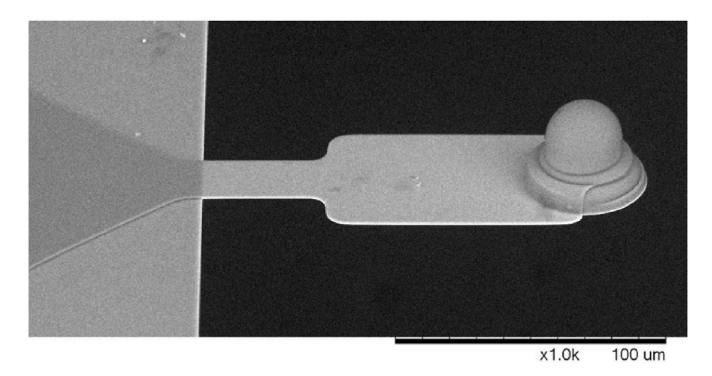


Fig. 2. SEM imaging of a previously used AFM probe Bruker SAA-SPH-10UM after cleaning with 3% Tergazyme.

matched the nominal specified by the manufacturer.

The cantilever's sensitivity was calibrated prior to performing cell measurements using a contact-based method and the Bruker JPK SPM software. The sensitivity was determined by collecting five force-displacement (F-D) curves on a glass slide that was glued to the surface of a 35 mm culture dish filled with the NFR solution (average of 5 measurements). Spring constant values provided by the manufacturer were manually entered in the JPK SPM software. Hydrogels with nominal indentation modulus of 8 kPa acquired from Matrigen (Irvine, CA, USA) were used as a reference to establish protocol for AFM experiments.

2.3. Bio-AFM experiments

2.3.1. Sample holder for oocytes

Oocytes were immobilized for Bio-AFM experiments using a sample holder fabricated from a 0.75 mm thick sheet of polyethylene terephthalate glycol (PETG) using a Boss Laser HP-2436 155 W laser cutter. The holder design was created using Adobe illustrator 2022 (Fig. 1 B). The holder was manually polished using wet sandpaper with a grit size of 3000 to remove sharp edges, washed with 70% ethanol and distilled water, dried and then securely attached to the bottom of a 35 mm culture dish with tape (Fig. 1 C).

2.3.2. Experimental procedure

The oocytes were stored at 4–6 $^{\circ}$ C and allowed to equilibrate with room temperature (25–27 $^{\circ}$ C) in NFR for 30 min prior to the start of imaging and force spectroscopy experiments. Oocytes were transferred into individual wells in the sample holder in a 35 mm Petri dish filled with NFR using a plastic pipette.

Oocytes with intact and removed VM were used for AFM measurements. Elastic property measurements were carried out in the Force Spectroscopy mode with a Z length of 5 μm and Z speed of 2 $\mu m/s$. F-D curves were captured on a $50\times50~\mu m$ area, using a 3x3 grid. A summary of the number of oocytes and maximum indentation force (setpoint) values used for data reported in the results section is provided in Table 1.

AtomicJ software (version 2.3.1; https://sourceforge.net/projects/jr obust/) (Hermanowicz et al., 2014) was used to fit the collected force spectroscopy data using Hertz and JKR models. The loading curve was used for the Hertz model fit, while the unloading curve was used for the

Table 1Number of oocytes and setpoint values used for live oocytes for the AFM force spectroscopy measurements.

VM	Oocyte's pole	Number of the oocytes measured	Setpoint, nN		
Intact	Animal	26	3	5	10
	Vegetal	20	3	5	10
Removed	Animal	5	0.1	0.5	1
	Vegetal	6	0.1	0.5	1

JKR model.

The surfaces of live oocytes were imaged in the QI mode at both poles. Areas of 50 \times 50 $\mu m, 25 \times 25 \ \mu m,$ and 10 \times 10 μm were scanned for each oocyte using the following parameters: setpoint 0.15 nN; Z length 3 $\mu m;$ Z speed 75 $\mu m/s;$ resolution 128x128 pixels. QI data were processed with JPK Data Processing software (Bruker, Berlin, Germany) to remove the general curvature of the cell with the following settings: plane fit (degree: 2), line leveling (degree: 2, pixel range: all pixels).

2.4. Finite element model

A three-dimensional finite element (FE) model with cyclic symmetry was developed using commercial finite element analysis software MSC Marc Mentat 2018 to simulate nanoindentation of live oocytes. The model comprises half of a spherical oocyte with a diameter of 1 mm modeled as an elastic deformable body and a rigid spherical indenter with a diameter of 20 μm . Although the actual shape of the indenter was cylindrical with a rounded tip, it was approximated as a sphere because the modeled indentation depth did not exceed the tip radius. Due to the lack of data on mechanical properties of organelles, the oocyte was represented in the model as a two-layered structure – VM layer surrounding the inner volume of the oocyte combining protoplasm and plasma membrane.

To quantify Young's modulus of the VM, several simulations were performed to obtain F-D curves comparable to the experimental. The $1\mbox{-}\mu m$ VM layer was meshed with four-node quadrilateral membrane elements and assigned Young's modulus values of 20, 40, and 60 MPa, and the Poisson's ratio of 0.49. Young's modulus of 0.2 kPa was used for the inner portion of the oocyte based on experiments conducted on oocytes without the VM; Poisson's ratio of 0.49 was assumed. The inner portion of the oocyte protoplasm was meshed using eight-node hexahedral solid elements. A preset indentation depth of 1 μm was employed to simulate the AFM indentation test.

2.5. Scanning electron microscopy

Oocytes were fixed in 4% glutaraldehyde in MBS solution, washed three times in NFR and post-fixed in 2% osmium tetroxide for 2 h. The oocytes were dehydrated by immersion for 30 min in a series of progressively higher ethanol concentrations (30%, 50%, 70%, 80%, 90%, 95%, 100 %), then chemically dried using the Tousimis Autosamdri-815 Series A critical point dryer (Tousimis Research Corporation, Rockville, MD). Samples were mounted on a 15 mm aluminum stub using double-sided carbon tape and conductive liquid silver paint. Oocytes were imaged with a tabletop scanning electron microscope Hitachi TM 1000 (Hitachi, Tokyo, Japan) using accelerating voltage 15 kV and emission current 60 mA at various magnifications.

2.6. Figure preparation

SEM image processing was implemented to enhance the visibility of the structure's components and improve overall image quality. The image enhancement was achieved by applying the auto contrast adjustment. In Fig. 1, the original raw images underwent cropping, and the scale bar was incorporated. All these modifications were conducted in Adobe Photoshop (2024).

2.7. Statistical methods

Normality of the outcome was assessed using the Shapiro-Wilk test (Royston, 1982a), (Royston, 1982b). Possible power transformations of the outcome to address non-Normality were assessed using Box-Cox (Venables and Ripley, 2002).

As the observations were not independent (e.g., there were up to 27 observations from each oocyte), linear mixed effects models were fit using maximum likelihood, using oocyte ID as a random intercept.

In each subset of the data, the final model was obtained by starting with the full pairwise interaction model and paring back using backwards selection based on the chi-square-test criterion; this is analogous to the F-test criterion during model selection among linear models with only fixed effects.

All pre-processing and analysis were performed in R version 4 (R Core Team, 2022); all linear mixed effects models were fit using the ImerTest package's extension (Kuznetsova et al., 2017) of the Ime4 package (Bates et al., 2015). The svglite package (Wickham et al., 2023) was used for image creation.

All p-values are reported to two significant digits, using scientific notation for very small p-values.

3. Results and discussion

In the present study, different factors such as structural variation (VM, oocytes poles) and experimental settings (maximum indentation force) were examined to determine the influence on the apparent Young's modulus of *Xenopus* oocytes as measured by nanoindentation. Our experimental plan was designed to capture measurements from fixed and live oocytes for protocol optimization and comparative analysis (Francis et al., 2010). Results for the fixed oocytes are presented in Supplementary material.

3.1. AFM and SEM imaging

The outer surface of the plasma membrane of the oocytes in invertebrates and amphibians is covered with the VM to block polyspermy (Sato, 2014). *Xenopus* oocyte's VM is an approximately 1-µm thick glycoprotein-rich extracellular layer covering the plasma membrane (Tian et al., 1997), (Sato, 2014). The VM develops between Stages II and IV where it reaches its maximum thickness (Dumont and Brummett, 1978)

Fig. 3 presents AFM images of the outer surface of the VM of a live oocyte acquired at different magnifications at the vegetal pole. These images reveal a porous structure characterized by an interconnected network of protein fibers with varying diameters. The pores are located close to each other and extend into the VM. The surface is uneven with well observed high and low areas.

AFM experiments conducted on live oocytes without VM were performed immediately after the VM removal. The lack of the VM resulted in the rapid loss of the characteristic spherical oocyte shape and gradually flattening of the cell. Attempts to perform AFM imaging of oocytes without the VM did not yield satisfactory results, possibly because the underlying layer of the microvilli might have been moving as the cell flattened during imaging.

The same interconnected network of fibers was observed via both AFM (Fig. 3) and SEM (Fig. 4) imaging. In the case of oocytes, the

presence of substantial pores limits the use of a smaller tip radius due to the likelihood of penetration into the cell rather than surface indentation. SEM images also unveil a layer of microvilli on the plasma membrane in the areas where the VM was accidently removed during the preparation process. Microvilli are around 1 μm in length and protrude from the plasma membrane toward the VM (Sonnleitner et al., 2002), a feature which can be distinctly observed in the SEM images (Fig. 4B and C). This microvillus layer may explain the challenges encountered during AFM imaging and force spectroscopy of oocytes following removal of the VM discussed in Section 3.2 – the microvilli adhere to the indenter tip and interfere with the tip's motion.

Taken together, these findings highlight that the acquisition of precise AFM measurements requires understanding of the specimen surface morphology. In the case of oocytes, the presence of substantial pores in the VM limits the use of a small tip radius (i.e. under $10~\mu m)$ due to the likelihood of penetration into the cell rather than surface indentation. Furthermore, the presence of a microvillus layer can explain difficulties in the AFM imaging and force spectroscopy measurements of the oocytes when the VM is removed.

3.2. AFM force spectroscopy

3.2.1. Probe selection and calibration

AFM tips are available in a variety of geometries including pyramidal (with three and four sides, each having different half-cone angles), spherical, and cylindrical. Previous studies have revealed that measurements of Young's modulus using pyramidal tips yield higher values compared to spherical probes (Dimitriadis et al., 2002), (Zemla et al., 2020), (Vargas-Pinto et al., 2013). Spherical tips are preferred due to cell inhomogeneity; they augment the contact area and prevent excessive penetration or probing into cellular gaps (Dimitriadis et al., 2002). Conversely, a sharp tip with a very small radius (1–5 nm) is more suitable for imaging of biological specimens.

The use of SAA-SPH-10UM with a 10 μ m tip radius for nanoindentation and elastic properties measurements can be justified based on the surface structure of the oocytes. Ensuring accurate measurements necessitates the tip size being notably larger than the diameter of fibers making up the VM and the gaps between the fibers (see Fig. 3). The largest commercially available spherical tip with a 10 μ m radius was employed for all the nanoindentation AFM experiments.

Prior to conducting any AFM experiments, it is crucial to perform calibration for both the cantilever's deflection sensitivity and spring constant. If the measurements are performed in liquid the calibration process must be performed in the same medium as the experiments. Investigating the potential sources of variability in the measurement of elastic moduli on soft materials, Schillers et al. (2017) demonstrated that cantilever calibration is a major contributor to measurement errors. Incorrect calibration of deflection sensitivity and spring constant results

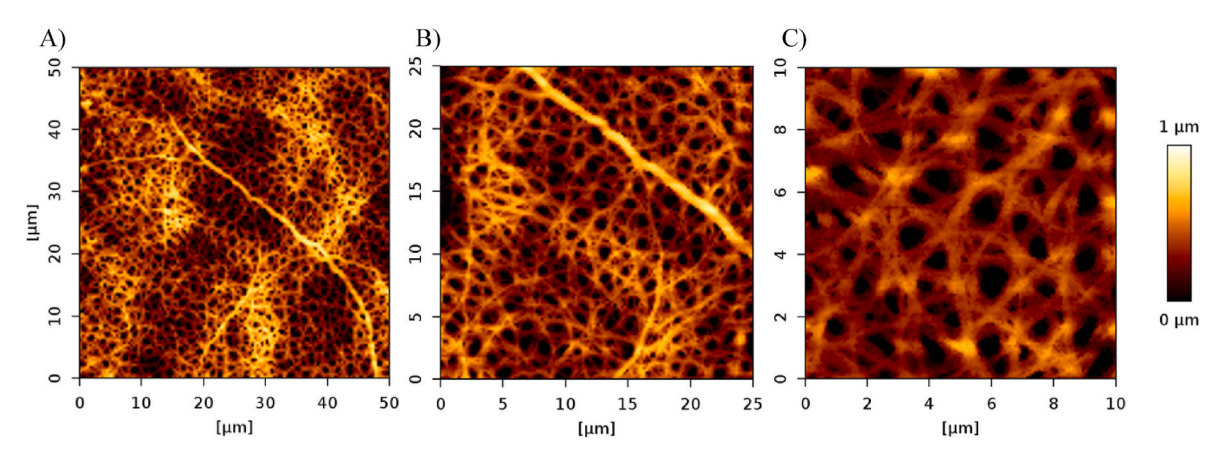


Fig. 3. AFM imaging of the vegetal pole of the live oocyte *Xenopus* oocyte's surface A) 50×50 μm area, B) 25×25 μm area, C) 10×10 μm area.

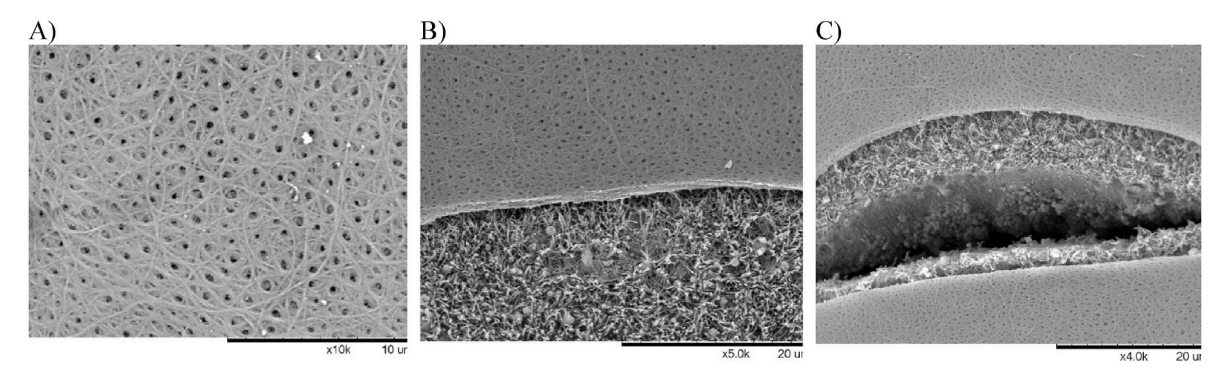


Fig. 4. SEM imaging of the fixed *Xenopus* oocyte A) Vitelline membrane surface, B) Vitelline membrane (top) and microvilli (bottom), C) a cracked oocyte surface reveals inner structure of microvilli and what appear to be lipid droplets (Dunning et al., 2014).

in inaccurate force and indentation values, leading to incorrect measurement of elastic properties from experimental data.

The deflection sensitivity should be measured before each experiment and after each laser re-alignment. This is important due to factors such as medium properties, the reflectivity of the coatings, and the precise location where the laser interacts with the cantilever (Gavara, 2017). The sensitivity calibration can be performed by contact-based or contact-free methods. However, the contact-free calibration method can be used only for rectangular cantilevers with uniform cross-section. In the case of contact-based method an F-D curve is measured on a hard surface such as glass and the linear segment of the slope is used to calculate the sensitivity.

Using the sensitivity measured during calibration, raw AFM measurements in volts can be converted into force measurements in Newtons (Zhou et al., 2021), (Cappella and Dietler, 1999). The tip-sample force can be expressed using Hooke's law (Li et al., 2018):

$$F = k\delta \tag{1}$$

where F is the applied force, k is the cantilever spring constant, and δ is the cantilever deflection.

The cantilever spring constant defines the relationship between the force applied and the resulting deflection. All cantilevers have a nominal spring constant however the exact value should be measured for each specific cantilever. The thermal noise method is usually used to calculate the spring constant (Norman et al., 2021). Some cantilevers come pre-calibrated by the manufacturer. In such case, spring constant calibration is not necessary, and the manufacturer-provided value can be directly utilized for experiments.

Stiffness of a specimen and the cantilever spring constant should be in the same range in order to perform a proper indentation (Gavara, 2017), (Norman et al., 2021). If the cantilever is too soft, it will not effectively indent the specimen, and if it is excessively stiff, specimen indentation might occur without any observable cantilever deflection (Norman et al., 2021). However, it is not always possible to predict the sample stiffness and initial cantilevers' testing is required.

3.2.2. Force spectroscopy data processing

The primary sources of errors in data processing lie in selecting the appropriate theoretical model for deriving elastic properties (Schillers et al., 2017) and determining the contact point between the tip and the sample (Zhou et al., 2021), (Kilpatrick et al., 2015).

Hertz and JKR models were used to analyze the F-D curves. The Hertz model is the most commonly used model for biological samples when a spherical indenter is used (Essmann et al., 2020), (Li et al., 2008), (Thomas et al., 2013). This model assumes that the sample is homogeneous, isotropic, and that deformation is linearly elastic (Kontomaris and Malamou, 2020). These assumptions should be considered when interpreting data obtained on biological samples which can be approximately considered as an elastic half space if the sample thickness is

relatively large compared to the indentation depth and relatively small compared to the probe radius (Kontomaris and Malamou, 2020). To avoid the influence of the underlying substrate, indentation depth should be less than 10% of the sample's thickness (Persch et al., 1994). Hertz model (Hertz) for a parabolic indenter shape:

$$F = \frac{4}{3} \frac{\sqrt{R_c E}}{1 - \nu^2} \delta^{3/2} \tag{2}$$

where *F* is the applied force, *E* is the Young's modulus, ν is the Poisson's ratio, R_c is the radius of tip curvature, and δ is the indentation depth.

F-D curves collected on *Xenopus* oocytes exhibit adhesion in the unloading portion (Fig. 5). However, the Hertz model performs the fit using the loading segment of F-D curve and does not account for adhesion forces (Krieg et al., 2018). Two widely accepted theoretical models that incorporate adhesion forces are Johnson–Kendall–Roberts (JKR) (Johnson et al., 1971) and Derjaguin–Muller–Toporov (DMT) (Derjaguin et al., 1975). JKR is suitable for soft samples, large tip radii, and high adhesive forces, while DMT is applicable to stiffer samples, small tip radii, and low adhesion forces (Efremov et al., 2015). The Tabor parameter μ (Tabor, 1977) determines the models' applicability and represents the ratio of adhesive and elastic interaction ranges (Willert et al., 2018), (Greenwood, 1997):

$$\mu = \sqrt[3]{\frac{R\Delta \gamma^2}{E^{*2}\varepsilon^3}} \tag{3}$$

$$R = \frac{R_1 R_2}{R_1 + R_2} \tag{4}$$

$$\frac{1}{E^*} = \frac{1 - \nu_1^2}{E_1} - \frac{1 - \nu_2^2}{E_2} \tag{5}$$

where $\Delta \gamma$ is the work of adhesion, ε is the equilibrium separation between the surfaces, R is the equivalent radius, E^* is the effective Young's modulus, R_i , E_i , ν_i , are the radii, the Young's moduli and the Poisson's ratio of two contacting spheres. ε is usually taken to be in between 0.3 and 0.5 nm (Efremov et al., 2015). Since the Young's modulus of the AFM tip is much greater than the oocytes' the term belonging to the tip in Equation (5) is relatively small and can be neglected.

JKR solution is valid for μ of 5 or higher (Greenwood, 1997). However, it is more accurate for large values of Tabor parameter (Ciavarella et al., 2019). For the F-D curves collected from the oocytes with intact VM calculated Tabor parameter was 3000 or more which is significantly higher than 5. Therefore, the data were additionally analyzed using the JKR model (Johnson et al., 1971):

$$F = \frac{4Ea^3}{3R(1 - v^2)} - 2\sqrt{2\pi \frac{E\gamma a^3}{1 - v^2}}$$
 (6)

where F is the applied force, E is the Young's modulus, v is the Poisson's ratio, a is a contact radius γ is the Dupré energy of adhesion, or

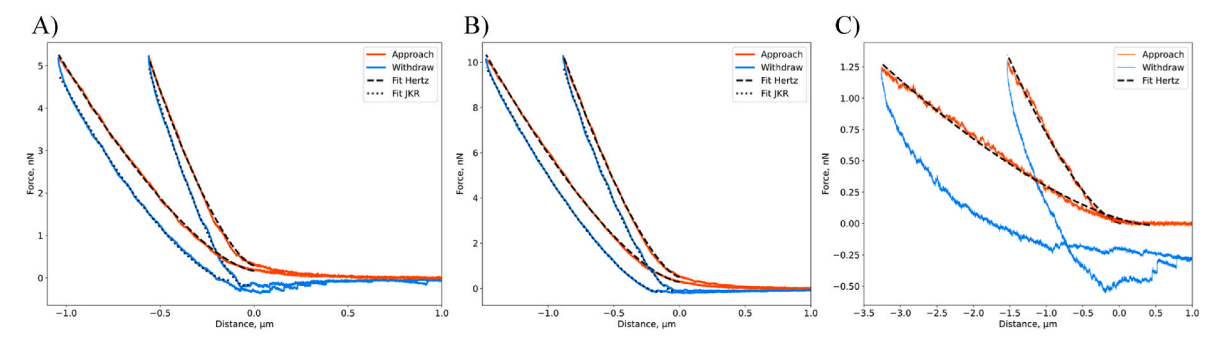


Fig. 5. Examples of force-displacement curves of live oocytes A) with intact VM measured at 5 nN setpoint (indention depth range $0.5-1~\mu m$); B) with intact VM measured at 10~nN setpoint (indention depth range $0.8-1.5~\mu m$); C) with removed VM measured at 1~nN (indentation depth range $1.6-3.5~\mu m$). Z length of $5~\mu m$ and Z speed of $2~\mu m/s$ were used to obtain all curves.

work of adhesion. For data analysis the cells were assumed to be incompressible, so the Poisson's ratio was taken to be 0.5 (Radmacher, 2002).

Examples of the force-displacement curves obtained from live oocytes with and without VM are shown on Fig. 5. The curves can be processed to extract Young's modulus, sample indentation depth, and amount of adhesion. F-D curves from the live oocytes with intact VM (Fig. 5 A and B) were fit by (Hertz) and JKR models. However, for the oocytes with removed VM collected F-D curves were irregular (Fig. 5 C). The retraction part of the curves shows a continuous adhesion and JKR fit could not be performed. The strong adhesion is attributed to the oocytes without VM being very soft and having a layer of microvilli that may stick to the tip and cause dragging. These F-D curves were analyzed only by Hertz model.

Fig. 6, and Fig. 7 present box plots illustrating log values of the apparent Young's modulus calculated from fitting the force-displacement curves. In each box plot, the horizontal line represents the median, while the box itself represents the interquartile range between the 25th and 75th percentiles. The whiskers extending from the lower and upper parts of the box signify the minimum and maximum values within each dataset. Outliers, denoted by circles, were identified

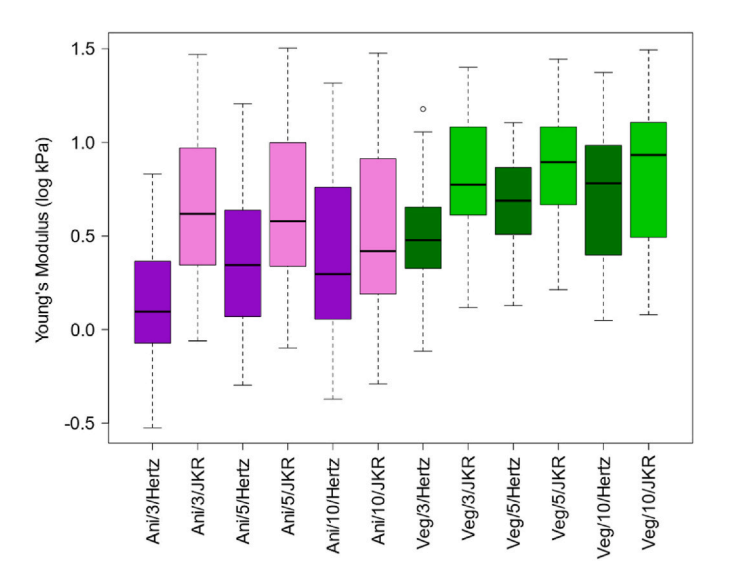


Fig. 6. Log values of the apparent Young's modulus of the live *Xenopus* oocytes with intact VM obtained at the animal and vegetal poles using three values of force setpoints based on the fit of force-displacement curves via two models (number of force-displacement curves used for each force setpoint is shown in the parentheses): animal pole/Hertz model (3 nN: 198, 5 nN: 209, 10 nN: 206), animal pole/JKR model (3 nN: 196, 5 nN: 209, 10 nN: 205), vegetal pole/Hertz model (3 nN: 144, 5 nN: 167, 10 nN: 173), vegetal pole/JKR model (3 nN: 143, 5 nN: 167, 10 nN: 173).

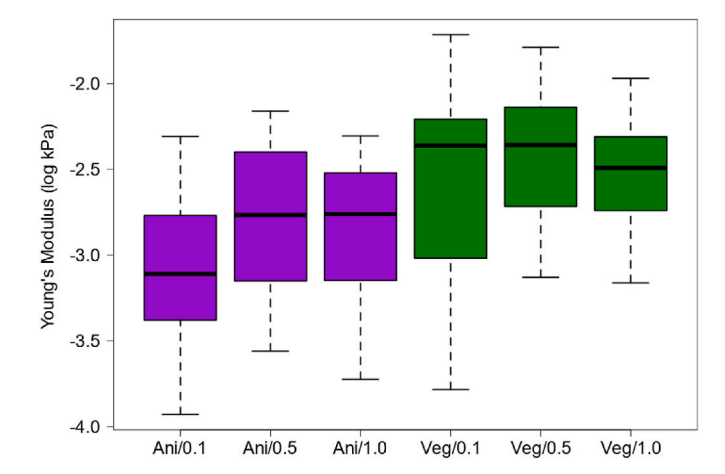


Fig. 7. Log values of the apparent Young's modulus of the live *Xenopus* oocytes without VM obtained at the animal and vegetal poles using three values of force setpoints based on the fit of force-displacement curves via the Hertz model (number of force-displacement curves used for each setpoint is shown in parentheses). animal pole (0.1 nN: 23, 0.5 nN: 32, 1 nN: 35), vegetal pole (0.1 nN: 26, 0.5 nN: 39, 1 nN: 44).

using the interquartile ranges (IQRs) method where any value 1.5 times the IQR above the third quartile or below the first quartile is flagged.

For both the Hertz and the JKR models, the Young's modulus of the live oocytes with intact VM lies in a range 0.8-5 kPa. Live oocytes with the removed VM were measured to have Young's modulus less than 0.2 kPa which is significantly softer than those with intact VM. The VM, which is primarily composed of glycoproteins, is a transparent flexible layer serving to maintain the oocyte's shape and volume, similar to how the rubber membrane of a water balloon functions. This has been confirmed by observations made during the removal of the VM, after which oocytes quickly lose their structure, become misshapen, and eventually disintegrate. The Young's modulus values of the live oocytes (Table 2, Table 3) agree with the values reported previously. Kelly et al. (1997) investigated the elastic properties of Xenopus oocytes by measuring intracellular pressure and cell volume. The authors reported specific elastance values for the oocytes with and without VM in the range 0-5.59 kPa and 0.15-1.03 kPa accordingly. The results of this study align with those of Kelly et al. (1997), even though different experimental techniques were employed.

Statistical analysis shows that the apparent Young's modulus values exhibited strong non-Normality (p-value = 1.6e-61). Box-Cox's suggested power transformation was approximately 0.1; for interpretability, a natural log transformation (Box-Cox power of 0) was chosen and used instead.

The F-D curves from the live oocytes without VM could not be fit

Table 2
Mean values of the apparent Young's moduli of live oocytes with intact VM (95% confidence intervals are shown in brackets).

Oocyte type	VM	Oocyte's pole	Apparent Young's modulus, kPa						
			3 nN		5 nN		10 nN		
			Hertz	JKR	Hertz	JKR	Hertz	JKR	
Live	Intact	Animal Vegetal	1.15 [1.02, 1.30] 1.69 [1.47, 1.95]	1.91 [1.69, 2.17] 2.35 [2.03, 2.71]	1.41 [1.25, 1.60] 1.94 [1.68, 2.24]	1.85 [1.63, 2.09] 2.38 [2.07. 2.75]	1.43 [1.26, 1.62] 2.05 [1.77, 2.36]	1.62 [1.43, 1.84] 2.27 [1.97, 2.62]	

Table 3
Mean values of the apparent Young's moduli of live oocytes with removed VM (95% confidence intervals are shown in brackets).

Oocyte type	VM	Oocyte's pole	Apparent Young's mo	dulus, kPa								
			0.1 nN		0.5 nN		1 nN					
			Hertz	JKR	Hertz	JKR	Hertz	JKR				
Live	Removed	Animal Vegetal	0.05 [0.04, 0.07] 0.07 [0.05, 0.09]	-	0.06 [0.05, 0.08] 0.08 [0.06, 0.11]	-	0.06 [0.04, 0.08] 0.08 [0.06, 0.11]	-				

with the JKR model. For these reasons, statistical analysis of the oocytes without VM was performed separately from the oocytes with the VM.

The final statistical model for live oocytes with intact VM data was the initial full pairwise interaction model (force setpoint: 3, 5, and 10 nN, pole: animal and vegetal, model: Hertz and JKR) as all pairwise interactions were significant: force-by-pole, p-value = 0.00019; force-by-model, p-value = 8.3e-77; pole-by-model, p-value = 1.4e-10.

The analysis showed a statistical difference between the JKR and the Hertz models. On average, the apparent Young's modulus mean values were approximately 23 % higher for the oocytes with VM when using the JKR model compared to the Hertz model. The JKR model appears to be less sensitive to the force applied and provides more consistent results across different forces. The Young's modulus values obtained from the JKR model also exhibit a wider range compared to the Hertz model. All data sets show that the apparent Young's modulus was higher at the vegetal pole compared to the animal pole for oocytes with the VM for a given setpoint.

In most cases, the force applied during the force spectroscopy measurements affects Young's modulus value: the higher the force setpoint, the higher the apparent Young's modulus. Exceptions were observed only for JKR model fit for the animal pole of the live oocytes with intact VM and the vegetal pole of the live oocytes with the removed VM. The observable impact of the force setpoint on the apparent Young's modulus for oocytes with intact VM may be attributed to the uneven surface of the VM. This effect is more pronounced for smaller forces, resulting in smaller indentation depths. Conversely, higher forces lead to increased probe-sample interaction, causing larger indentations and reduced sensitivity to surface structure. Another potential factor contributing to these observations is the influence of adhesion and the inhomogeneity of the oocyte's structure. The higher force results in deeper indentation and therefore contribution of the underlying biological structures such as the actin cortex and the cytoskeleton might be the reason for the increase in Young's modulus.

In the case of statistical analysis of the live oocytes without VM, the full pairwise interaction model only has three terms: a main effect for force setpoint (0.1, 0.5, and 1 nN), a main effect for pole (animal and vegetal) and their interaction. The force-by-pole interaction was not significant (p-value = 0.86). After removing the interaction from the model, the main effect of pole was not significant (p-value = 0.085). Which indicates that there is no statistic difference between the apparent Young's modulus measured at animal and vegetal poles of the live oocytes without VM. After removing the main effect for pole, the main effect of force was significant (p-value = 0.00031).

We performed stratified analyses to further investigate the observed interactions among force, pole, and model. Based on these analyses, the only case where there was no effect in one substratum vs another was

when looking at force measurements performed on the vegetal pole of live cells with intact VM when comparing JKR and Hertz models.

Tables 2 and 3 summarize the results of the average values of the apparent Young's modulus measured for the oocytes with and without VM. The average values were calculated from all F-D curves collected for a specific force (multiple oocytes).

3.3. Finite element analysis

AFM nanoindentation was simulated via FE analysis to estimate the order of magnitude of the VM's Young's modulus. The comparison between simulated F-D curves, using three different Young's moduli for the VM (20, 40, and 60 MPa), and experimental curves measured at 5 nN setpoint is illustrated in Fig. 8. As expected, the maximum force increases with increasing stiffness of the VM. The simulated F-D curves for VM Young's modulus in the range of 20–60 MPa resemble some experimental results in terms of curve shape, maximum indentation force, and indentation depth. Although we compared the simulated results only to F-D curves with an indentation depth of around 0.9–1 μ m, other curves representing higher apparent stiffness did not fit these simulation results. The higher apparent stiffness may result from a thicker VM in some oocytes or certain areas of oocytes.

The FE model behavior using two different element types for the VM, membrane and shell elements, was compared to assess the significance of bending stiffness in the VM. Ultimately, membrane elements were selected to represent the VM following validation against experimental

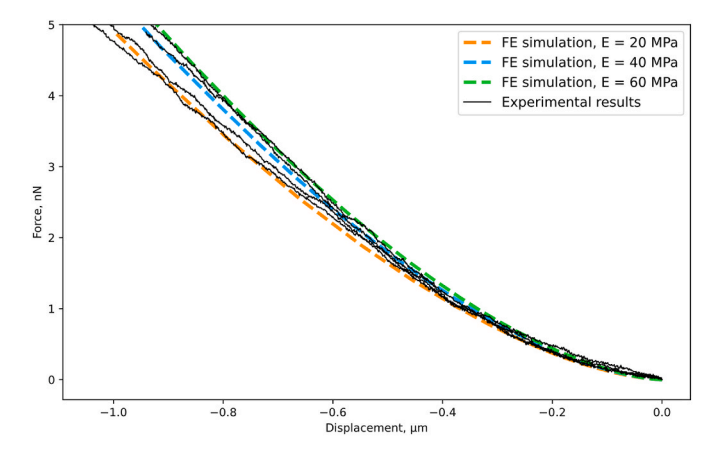


Fig. 8. Comparison of simulated F-D curve with the AFM experimental curves. Simulations results represent F-D curve for different Young's modulus of the VM: 20, 40, and 60 MPa.

data, which indicates that contribution of the VM's bending stiffness is negligible. Results of these simulations are provided in the Supplementary Material.

4. Conclusions

Combination of AFM and SEM imaging enabled a deeper understanding of the sample surface in the context of our experimental design. The porous nature of the VM required the use of a large radius AFM tip (10 μ m) since a smaller radius could not effectively engage with the surface of the sample.

This study focused on investigating the impact of the VM, the oocyte surface region (animal vs vegetal pole), and maximum indentation force on the apparent Young's modulus of the *Xenopus laevis* oocytes. The analysis revealed that mean Young's modulus values measured at the vegetal pole were consistently higher than at the animal for all oocytes with intact VM. However, the effect of VM removal was more substantial. The apparent Young's modulus of live oocytes with the VM was substantially higher than that of live oocytes with the VM removed, indicating that the VM is one of the main structural components responsible for stiffness of the oocyte. This conclusion was further supported by FE analysis. The Young's modulus of the VM was estimated to be in a range 20–60 MPa, which is five orders of magnitude higher than the oocytes without the VM.

For all oocytes with intact VM the JKR model consistently yielded higher Young's modulus values compared to the Hertz model. For both models, the effect of force was observed to be significant (higher force resulted in higher Young's modulus). However, the mean values of the Young's modulus calculated with the JKR model were found to be less sensitive to the applied force.

Our findings indicate that choice of mechanical model for fitting force-displacement curves, maximum indentation force, and location of indentation are all important and have a significant effect on measured mechanical properties. Therefore, careful experimental design is essential to accurately address the specific questions targeted in a study.

Future studies should focus on exploring mechanical properties of the isolated VM and other components within oocytes, such as the plasma membrane, actin cortex, and protoplasm. These investigations should evaluate the individual contribution of these components to the overall mechanical properties of oocytes. Diverse experimental techniques (bulk tension/compression) may be necessary to assess the overall elastic properties of oocytes effectively. Furthermore, the presented FE model can be further improved by incorporating additional oocyte components (e.g. plasma membrane, actin cortex etc.) and their experimentally measured mechanical properties.

Statement on the use of generative AI tools

During the preparation of this work the authors used ChatGPT 3.5 in order to improve the language of the initial draft. After using this tool, the authors reviewed and edited the content as needed and take full responsibility for the content of the publication.

CRediT authorship contribution statement

Tatiana Kardashina: Writing – review & editing, Writing – original draft, Visualization, Methodology, Investigation, Formal analysis. **Elba E. Serrano:** Writing – review & editing, Supervision, Resources, Methodology, Funding acquisition, Conceptualization. **John A. Dawson:** Writing – review & editing, Visualization, Methodology, Formal analysis. **Borys Drach:** Writing – review & editing, Supervision, Methodology, Conceptualization.

Declaration of competing interest

The authors declare the following financial interests/personal

relationships which may be considered as potential competing interests:

Elba E Serrano reports financial support was provided by National Science Foundation. Borys Drach reports financial support was provided by National Science Foundation. If there are other authors, they declare that they have no known competing financial interests or personal relationships that could have appeared to influence the work reported in this paper.

Data availability

Data will be made available on request.

Acknowledgments

This material is based upon work supported by the National Science Foundation under grants No. CMMI-2011220, No. DBI-2117045 and MRI CMMI-2215982. We thank Dr. Belteton and Batool Al-Khatib at the Microscopic Imaging Core Suite for their guidance on oocyte sample preparation and SEM imaging.

Appendix A. Supplementary data

Supplementary data to this article can be found online at $\frac{https:}{doi.}$ org/10.1016/j.jmbbm.2024.106648.

References

- Ayad, N.M.E., Kaushik, S., Weaver, V.M., 2019. Tissue mechanics, an important regulator of development and disease. Philos. Trans. R. Soc. B Biol. Sci. 374 (1779), 20180215 https://doi.org/10.1098/rstb.2018.0215.
- Bates, D., Mächler, M., Bolker, B., Walker, S., 2015. Fitting linear mixed-effects models using lme4. J. Stat. Software 67 (1). https://doi.org/10.18637/jss.v067.i01.
- Battistella, A., et al., 2022. Atomic force spectroscopy-based essay to evaluate oocyte postovulatory aging. Bioeng. Transl. Med. 7 (3), e10294 https://doi.org/10.1002/btm2.10294
- Braet, F., Rotsch, C., Wisse, E., Radmacher, M., 1998. Comparison of fixed and living liver endothelial cells by atomic force microscopy. Appl. Phys. Mater. Sci. Process 66 (7), S575–S578. https://doi.org/10.1007/s003390051204.
- Cappella, B., Dietler, G., 1999. Force-distance curves by atomic force microscopy. Surf. Sci. Rep. 34 (1–3), 1–104. https://doi.org/10.1016/S0167-5729(99)00003-5.
- Ciavarella, M., Joe, J., Papangelo, A., Barber, J.R., 2019. The role of adhesion in contact mechanics. J. R. Soc. Interface 16 (151), 20180738. https://doi.org/10.1098/ rsif.2018.0738.
- Codan, B., Martinelli, V., Mestroni, L., Sbaizero, O., 2013. Atomic force microscopy of 3T3 and SW-13 cell lines: an investigation of cell elasticity changes due to fixation. Mater. Sci. Eng. C 33 (6), 3303–3308. https://doi.org/10.1016/j.msec.2013.04.009.
- Cross, S.E., Jin, Y.-S., Rao, J., Gimzewski, J.K., 2007. Nanomechanical analysis of cells from cancer patients. Nat. Nanotechnol. 2 (12), 780–783. https://doi.org/10.1038/ nnano.2007.388.
- Dahl, K.N., Engler, A.J., Pajerowski, J.D., Discher, D.E., 2005. Power-law rheology of isolated nuclei with deformation mapping of nuclear substructures. Biophys. J. 89 (4), 2855–2864. https://doi.org/10.1529/biophysj.105.062554.
- Daily, B., Elson, E.L., Zahalak, G.I., 1984. Cell poking. Determination of the elastic area compressibility modulus of the erythrocyte membrane. Biophys. J. 45 (4), 671–682. https://doi.org/10.1016/S0006-3495(84)84209-5.
- Darling, E.M., Zauscher, S., Guilak, F., 2006. Viscoelastic properties of zonal articular chondrocytes measured by atomic force microscopy. Osteoarthritis Cartilage 14 (6), 571–579. https://doi.org/10.1016/j.joca.2005.12.003.
- Daza, R., et al., 2019. Comparison of cell mechanical measurements provided by atomic force microscopy (AFM) and micropipette aspiration (MPA). J. Mech. Behav. Biomed. Mater. 95, 103–115. https://doi.org/10.1016/j.jmbbm.2019.03.031.
- Derjaguin, B.V., Muller, V.M., Toporov, Yu P., 1975. Effect of contact deformations on the adhesion of particles. J. Colloid Interface Sci. https://doi.org/10.1016/0021-9797(75)90018-1.
- Dimitriadis, E.K., Horkay, F., Maresca, J., Kachar, B., Chadwick, R.S., 2002.
 Determination of elastic moduli of thin layers of soft material using the atomic force microscope. Biophys. J. 82 (5), 2798–2810. https://doi.org/10.1016/S0006-3495 (02)75620-8.
- Dumont, J.N., Brummett, A.R., 1978. Oogenesis inXenopus laevis (Daudin). V. Relationships between developing oocytes and their investing follicular tissues. J. Morphol. 155 (1), 73–97. https://doi.org/10.1002/jmor.1051550106.
- Dunning, K.R., Russell, D.L., Robker, R.L., 2014. Lipids and oocyte developmental competence: the role of fatty acids and β-oxidation. Reproduction 148 (1), R15–R27. https://doi.org/10.1530/REP-13-0251.
- Efremov, Yu M., Bagrov, D.V., Kirpichnikov, M.P., Shaitan, K.V., 2015. Application of the Johnson–Kendall–Roberts model in AFM-based mechanical measurements on cells and gel. Colloids Surf. B Biointerfaces 134, 131–139. https://doi.org/10.1016/j. colsurfb.2015.06.044.

- Elad, D., Jaffa, A.J., Grisaru, D., 2020. Biomechanics of early life in the female reproductive tract. Physiology 35 (2), 134–143. https://doi.org/10.1152/ physiol.00028.2019.
- Essmann, C.L., et al., 2020. Mechanical properties measured by atomic force microscopy define health biomarkers in ageing C. elegans. Nat. Commun. 11 (1), 1043. https:// doi.org/10.1038/s41467-020-14785-0.
- Francis, L.W., et al., 2010. Optimized sample preparation for high-resolution AFM characterization of fixed human cells. J. Microsc. 240 (2), 111–121. https://doi.org/ 10.1111/j.1365-2818.2010.03392.x.
- Gavara, N., 2017. A beginner's guide to atomic force microscopy probing for cell mechanics: gavara. Microsc. Res. Tech. 80 (1), 75–84. https://doi.org/10.1002/ iont.22776
- Greenwood, J.A., 1997. Adhesion of elastic spheres. Proc. R. Soc. Lond. Ser. Math. Phys. Eng. Sci. 453 (1961), 1277–1297. https://doi.org/10.1098/rspa.1997.0070.
- Hermanowicz, P., Sarna, M., Burda, K., Gabryś, H., 2014. AtomicJ: an open source software for analysis of force curves. Rev. Sci. Instrum. 85 (6), 063703 https://doi. org/10.1063/1.4881683.
- H. Heriz, "Über die Berührung fester elastischer Körper," J. für die Reine Angewandte Math. (Crelle's J.), 1881, doi: 10.1515/9783112342404-004.
- Jaalouk, D.E., Lammerding, J., 2009. Mechanotransduction gone awry. Nat. Rev. Mol. Cell Biol. 10 (1), 63–73. https://doi.org/10.1038/nrm2597.
- Johnson, K.L., Kendall, K., Roberts, A.D., 1971. Surface energy and the contact of elastic solids. Proc. R. Soc. Lond. Ser. Math. Phys. Sci. 324 (1558), 301–313.
- Kelly, S.M., Jia, Y.L., Macklem, P.T., 1997. Measurement of elastic properties of Xenopus oocytes. Comp. Biochem. Physiol. A Physiol. 118 (3), 607–613. https://doi.org/ 10.1016/S0300-9629(96)00483-5
- Kilpatrick, J.I., Revenko, I., Rodriguez, B.J., 2015. Nanomechanics of cells and biomaterials studied by atomic force microscopy. Adv. Healthcare Mater. 4 (16), 2456–2474. https://doi.org/10.1002/adhm.201500229.
- Kontomaris, S.V., Malamou, A., 2020. Hertz model or Oliver & Pharr analysis? Tutorial regarding AFM nanoindentation experiments on biological samples. Mater. Res. Express 7 (3), 033001. https://doi.org/10.1088/2053-1591/ab79ce.
- Kort, J., Behr, B., 2017. Biomechanics and developmental potential of oocytes and embryos. Fertil. Steril. 108 (5), 738–741. https://doi.org/10.1016/j. fertnstert.2017.09.016.
- Krieg, M., et al., 2018. Atomic force microscopy-based mechanobiology. Nat. Rev. Phys. 1 (1), 41–57. https://doi.org/10.1038/s42254-018-0001-7.
- Kuznetsova, A., Brockhoff, P.B., Christensen, R.H.B., 2017. ImerTest package: tests in linear mixed effects models. J. Stat. Software 82 (13). https://doi.org/10.18637/jss. v082.i13.
- Larabell, C.A., Chandler, D.E., 1989. The coelomic envelope of Xenopus laevis eggs: a quick-freeze, deep-etch analysis. Dev. Biol. 131 (1), 126–135. https://doi.org/ 10.1016/S0012-1606(89)80044-2.
- Li, Q.S., Lee, G.Y.H., Ong, C.N., Lim, C.T., 2008. AFM indentation study of breast cancer cells. Biochem. Biophys. Res. Commun. 374 (4), 609–613. https://doi.org/10.1016/ j.bbrc.2008.07.078.
- Li, M., Liu, L., Xi, N., Wang, Y., 2018. Atomic force microscopy studies on cellular elastic and viscoelastic properties. Sci. China Life Sci. 61 (1), 57–67. https://doi.org/ 10.1007/s11427-016-9041-9.
- Mathur, A.B., Collinsworth, A.M., Reichert, W.M., Kraus, W.E., Truskey, G.A., 2001. Endothelial, cardiac muscle and skeletal muscle exhibit different viscous and elastic properties as determined by atomic force microscopy. J. Biomech. 34 (12), 1545–1553. https://doi.org/10.1016/S0021-9290(01)00149-X.
- McConnaughey, W.B., Petersen, N.O., 1980. Cell poker: an apparatus for stress-strain measurements on living cells. Rev. Sci. Instrum. 51 (5), 575–580. https://doi.org/ 10.1063/1.1136256.
- Méndez-Vilas, A., Díaz, J. (Eds.), 2010. Microscopy: Science, Technology, Applications and Education. Badajoz. Formatex Research Center.
- Mowry, K.L., 2020. Using the Xenopus oocyte toolbox. Cold Spring Harb. Protoc. 2020 (4) https://doi.org/10.1101/pdb.top095844 pdb.top.095844.
- Norman, M.D.A., Ferreira, S.A., Jowett, G.M., Bozec, L., Gentleman, E., 2021. Measuring the elastic modulus of soft culture surfaces and three-dimensional hydrogels using atomic force microscopy. Nat. Protoc. 16 (5), 2418–2449. https://doi.org/10.1038/ ex1506.021.00405.4
- Persch, G., Born, Ch, Utesch, B., 1994. Nano-hardness investigations of thin films by an atomic force microscope. Microelectron. Eng. 24 (1–4), 113–121. https://doi.org/
- Petersen, N.O., McConnaughey, W.B., Elson, E.L., 1982. Dependence of locally measured cellular deformability on position on the cell, temperature, and cytochalasin B. Proc. Natl. Acad. Sci. USA 79 (17), 5327–5331. https://doi.org/10.1073/ pnas.79.17.5327.
- R Core Team, 2022. R: A Language and Environment for Statistical Computing. R Foundation for Statistical Computing, Vienna, Austria [Online]. Available: https://www.R-project.org/.
- Radmacher, M., 2002. Measuring the elastic properties of living cells by the atomic force microscope. In: Methods in Cell Biology, 68. Elsevier, pp. 67–90. https://doi.org/ 10.1016/S0091-679X(02)68005-7.

- Rico, F., Roca-Cusachs, P., Gavara, N., Farré, R., Rotger, M., Navajas, D., 2005. Probing mechanical properties of living cells by atomic force microscopy with blunted pyramidal cantilever tips. Phys. Rev. E 72 (2), 021914. https://doi.org/10.1103/ PhysRevE 72 021914
- Rosenbluth, M.J., Lam, W.A., Fletcher, D.A., 2006. Force microscopy of nonadherent cells: a comparison of leukemia cell deformability. Biophys. J. 90 (8), 2994–3003. https://doi.org/10.1529/biophysi.105.067496.
- Royston, J.P., 1982a. An extension of Shapiro and wilk's W test for normality to large samples. Appl. Stat. 31 (2), 115. https://doi.org/10.2307/2347973.
- Royston, J.P., 1982b. Algorithm AS 181: the W test for normality. Appl. Stat. 31 (2), 176. https://doi.org/10.2307/2347986.
- Sackmann, E., 1994. Intra- and extracellular macromolecular networks: physics and biological function. Macromol. Chem. Phys. 195 (1), 7–28. https://doi.org/10.1002/ macp.1994.021950103.
- Salbreux, G., Charras, G., Paluch, E., 2012. Actin cortex mechanics and cellular morphogenesis. Trends Cell Biol. 22 (10), 536–545. https://doi.org/10.1016/j.
- Sato, K., 2014. Transmembrane signal transduction in oocyte maturation and fertilization: focusing on Xenopus laevis as a model animal. Int. J. Mol. Sci. 16 (1), 114–134. https://doi.org/10.3390/ijms16010114.
- Schillers, H., et al., 2017. Standardized nanomechanical atomic force microscopy procedure (SNAP) for measuring soft and biological samples. Sci. Rep. 7 (1), 5117. https://doi.org/10.1038/s41598-017-05383-0.
- Shah, J.S., Sabouni, R., Cayton Vaught, K.C., Owen, C.M., Albertini, D.F., Segars, J.H., 2018. Biomechanics and mechanical signaling in the ovary: a systematic review. J. Assist. Reprod. Genet. 35 (7), 1135–1148. https://doi.org/10.1007/s10815-018-1180-y.
- Sonnleitner, A., Mannuzzu, L.M., Terakawa, S., Isacoff, E.Y., 2002. Structural rearrangements in single ion channels detected optically in living cells. Proc. Natl. Acad. Sci. USA 99 (20), 12759–12764. https://doi.org/10.1073/pnas.192261499.
- Suresh, S., 2007. Biomechanics and biophysics of cancer cells. Acta Mater. 55 (12), 3989-4014. https://doi.org/10.1016/j.actamat.2007.04.022.
- Suresh, S., et al., 2005. Connections between single-cell biomechanics and human disease states: gastrointestinal cancer and malaria. Acta Biomater. 1 (1), 15–30. https://doi. org/10.1016/j.actbio.2004.09.001.
- Tabor, D, 1977. Surface forces and surface interactions. J. Colloid Interface Sci. 58 (1) https://doi.org/10.1016/0021-9797(77)90366-6. ISSN 0021-9797.
- Thomas, G., Burnham, N.A., Camesano, T.A., Wen, Q., 2013. Measuring the mechanical properties of living cells using atomic force microscopy. J. Vis. Exp. (76), 50497 https://doi.org/10.3791/50497.
- Tian, J., Gong, H., Thomsen, G.H., Lennarz, W.J., 1997. Gamete interactions in Xenopus laevis: identification of sperm binding glycoproteins in the egg vitelline envelope. J. Cell Biol. 136 (5), 1099–1108. https://doi.org/10.1083/jcb.136.5.1099.
- Valentine, M.T., Perlman, Z.E., Mitchison, T.J., Weitz, D.A., 2005. Mechanical properties of Xenopus egg cytoplasmic extracts. Biophys. J. 88 (1), 680–689. https://doi.org/ 10.1529/biophysi.104.048025.
- Vargas-Pinto, R., Gong, H., Vahabikashi, A., Johnson, M., 2013. The effect of the endothelial cell cortex on atomic force microscopy measurements. Biophys. J. 105 (2), 300–309. https://doi.org/10.1016/j.bpj.2013.05.034.
- Venables, W.N., Ripley, B.D., 2002. Modern Applied Statistics with S. Fourth Edition. Springer.
- Wickham, H., Henry, L., Pedersen, T., Luciani, T., Decorde, M., Lise, V., 2023. svglite: an 'SVG' graphics device. R package version 2.1.3. https://CRAN.R-project.org/package-svglite
- Willert, E., Lyashenko, I.A., Popov, V.L., 2018. Influence of the Tabor parameter on the adhesive normal impact of spheres in Maugis–Dugdale approximation. Comput. Part. Mech. 5 (3), 313–318. https://doi.org/10.1007/s40571-017-0170-7.
- Wozniak, M.A., Chen, C.S., 2009. Mechanotransduction in development: a growing role for contractility. Nat. Rev. Mol. Cell Biol. 10 (1), 34–43. https://doi.org/10.1038/ psg. 320.
- Wu, P.-H., et al., 2018. A comparison of methods to assess cell mechanical properties. Nat. Methods 15 (7), 491–498. https://doi.org/10.1038/s41592-018-0015-1.
- Xu, W., Mezencev, R., Kim, B., Wang, L., McDonald, J., Sulchek, T., 2012. Cell stiffness is a biomarker of the metastatic potential of ovarian cancer cells. PLoS One 7 (10), e46609. https://doi.org/10.1371/journal.pone.0046609.
- Yanez, L.Z., Han, J., Behr, B.B., Pera, R.A.R., Camarillo, D.B., 2016. Human oocyte developmental potential is predicted by mechanical properties within hours after fertilization. Nat. Commun. 7 (1), 10809 https://doi.org/10.1038/ncomms10809.
- Yen, M.-H., Chen, Y.-H., Liu, Y.-S., Lee, O.K.-S., 2020. Alteration of Young's modulus in mesenchymal stromal cells during osteogenesis measured by atomic force microscopy. Biochem. Biophys. Res. Commun. 526 (3), 827–832. https://doi.org/ 10.1016/j.bbrc.2020.03.146.
- Zemła, J., et al., 2020. Indenting soft samples (hydrogels and cells) with cantilevers possessing various shapes of probing tip. Eur. Biophys. J. 49 (6), 485–495. https://doi.org/10.1007/s00249-020-01456-7.
- Zhou, G., Zhang, B., Tang, G., Yu, X.-F., Galluzzi, M., 2021. Cells nanomechanics by atomic force microscopy: focus on interactions at nanoscale. Adv. Phys. X 6 (1), 1866668. https://doi.org/10.1080/23746149.2020.1866668.